

Article

Histomorphometry of Ossification in Functionalised Ceramics with Tripeptide Arg-Gly-Asp (RGD): An In Vivo Study

Filippo Migliorini ^{1,†} , Hanno Schenker ^{1,†}, Nicola Maffulli ^{2,3,4,*} , Frank Hildebrand ¹ and Jörg Eschweiler ¹

¹ Department of Orthopaedic, Trauma and Reconstructive Surgery, RWTH University Hospital, 52074 Aachen, Germany; migliorini.md@gmail.com (F.M.); hschenker@ukaachen.de (H.S.); fhildebrand@ukaachen.de (F.H.); joeschweiler@ukaachen.de (J.E.)

² Department of Medicine, Surgery and Dentistry, University of Salerno, 84081 Baronissi, Italy

³ School of Pharmacy and Bioengineering, Keele University Faculty of Medicine, Stoke on Trent ST4 7QB, UK

⁴ Barts and The London School of Medicine and Dentistry, Centre for Sports and Exercise Medicine, Mile End Hospital, Queen Mary University of London, London E1 4DG, UK

* Correspondence: n.maffulli@qmul.ac.uk

† These authors contributed equally to this work and share the first authorship.

Abstract: The present study investigated the osseointegration promoted by functionalised ceramics with peptide Arg-Gly-Asp (RGD) in a rabbit model in vivo. Histomorphometry of the RGD functionalised ceramic implants was conducted by a trained pathologist to quantify the amount of mature and immature ossification at the bone interface, and then compared to titanium alloy implants. The region of interest was the area surrounding the implant. The percentage of ROI covered by osteoid implant contact and mature bone implant contact were assessed. The presence of bone resorption, necrosis, and/or inflammation in the areas around the implant were quantitatively investigated. All 36 rabbits survived the experimental period of 6 and 12 weeks. All implants remained in situ. No necrosis, bone resorption, or inflammation were identified. At 12 weeks follow-up, the overall mean bone implant contact ($p = 0.003$) and immature osteoid contact ($p = 0.03$) were improved compared to the mean values evidenced at 6 weeks. At 6 weeks follow-up, the overall osteoid implant contact was greater in the RGD enhanced group compared to the titanium implant ($p = 0.01$). The other endpoints of interest were similar between the two implants at all follow-up points ($p \geq 0.05$). Functionalised ceramics with peptide RGD promoted ossification in vivo. The overall osteoid and bone implant contact improved significantly from 6 to 12 weeks. Finally, RGD enhanced ceramic promoted faster osteoid implant contact in vivo than titanium implants. Overall, the amount of ossification at 12 weeks is comparable with the titanium implants. No necrosis, bone resorption, or inflammation were observed in any sample.

Keywords: functionalised ceramic; RGD; implantology; ossification



Citation: Migliorini, F.; Schenker, H.; Maffulli, N.; Hildebrand, F.; Eschweiler, J. Histomorphometry of Ossification in Functionalised Ceramics with Tripeptide Arg-Gly-Asp (RGD): An In Vivo Study. *Life* **2022**, *12*, 761. <https://doi.org/10.3390/life12050761>

Academic Editor: Peter Zioupos

Received: 1 April 2022

Accepted: 16 May 2022

Published: 20 May 2022

Publisher's Note: MDPI stays neutral with regard to jurisdictional claims in published maps and institutional affiliations.



Copyright: © 2022 by the authors. Licensee MDPI, Basel, Switzerland. This article is an open access article distributed under the terms and conditions of the Creative Commons Attribution (CC BY) license (<https://creativecommons.org/licenses/by/4.0/>).

1. Introduction

Metallic implants are commonly used in musculoskeletal medicine. Given its biocompatibility and ossification potential, alongside relatively lower elasticity module and breaking strength, titanium is the most commonly used component of prosthetic implants [1–5]. However, titanium alloys may be responsible for hypersensitivity reactions, which may compromise implant longevity. When low-grade infection and other mechanical problems have been excluded, symptoms, such as pruritus, pain, effusion, erythema, and hypersensitivity reactions, should be taken into consideration [6]. Ions released by corrosion of metallic wear debris may impair ossification and metal particles can be found in the soft tissues surrounding the implant [7]. Particles and ions may become clinically relevant for sensitive patients. According to the 2016 Australian Arthroplasty Register, approximately 2% of revision TKAs are consequent to metal-related pathology [8]. In selected patients with hypersensitivity, non-metallic implants may be used with unpredictable results [9]. Current

research to develop alternatives to metal alloys is ongoing. In this context, ceramic implants offer several advantages: hardness and wear resistance; light weight; low modulus of elasticity; outstanding resistance to creep and compressive stress; and lack of artefacts at imaging [10–12]. Although it reduces particle release, the risk of rejection, and implant loosening, the biological inactivity of ceramic impairs the integration of the implant into the surrounding bone tissue [13–15].

We developed a coating methodology using high-performance ceramic biologically activated with a silicate coating on alumina (Al_2O_3) and coated with peptide Arg-Gly-Asp (RGD) [16–19]. This study investigated the osseointegration provided by ceramic functionalised with the RGD peptide *in vivo*. The peptide RGD, derived from fibronectin in the extracellular matrix, increases cell attachment with optimal stable bioactivity and has been postulated to enhance implant osseointegration [20–22]. To the best of our knowledge, no previous study has evaluated the osseointegration of activated ceramic implants enhanced with the RGD peptide. We, therefore, conducted histomorphometry studies around the distal, proximal, medial, and lateral sides of the RGD functionalised ceramic implants to quantify the amount of mature and immature ossification within the bone interface. We hypothesised that ceramic implants functionalised with the RGD peptide promote ossification and transplant integration. The osseointegration of RGD functionalised ceramics was compared to that provided by commercially available titanium alloy implants.

2. Material and Methods

2.1. Sample Preparation

Sandblasted titanium implants by Fa. Zimmer Biomet Deutschland GmbH (Neu-Ulm, Germany), with a diameter of 5.5 mm and length of 8 mm, were used for surgery. Activated ceramics were manufactured at the Department of Dental Materials Science and Biomaterial Research of the RWTH University Aachen, Germany. The process to obtain active ceramic samples has been described in detail [23]. Briefly, standard Al_2O_3 ceramic based cylinders were used. Plasma-enhanced chemical vapor deposition (PE-CVD) was performed to facilitate the coupling of stable organosilane monolayers on the monolithic Al_2O_3 ceramic based cylinders [24]. These cylinders were activated using silicon suboxide (SiO_x), which was deposited on the polished and Al_2O_3 ceramic based cylinders [25]. Activated ceramic cylinders were then air-dried, cured at 80° for 45 min, and stored in liquid nitrogen until use. The day before surgery, the activated ceramics were coated with RGD. RGD was purified using size exclusion centrifugation and coated over the activated ceramic cylinders using crosslinkers bis(succinimidyl) suberate (BS3, Thermo Fisher, Woodward Austin, TX, USA) as received [26]. Purity was confirmed via antibody detection (monoclonal clone antibody anti-RGD, R&D Systems, Germany) and osteogenic induction capabilities via Human Mesenchymal Stem Cells (hMSC) [27]. Protein concentration was measured using a bicinchoninic acid assay (BCA, Thermo Fisher, Woodward Austin, TX, USA) [28]. All experiments were performed in triplicate. More detailed information on the RGD coating process can be found in a previous report [29].

2.2. Surgical Procedure

This study was conducted in 2016 according to the Animal Welfare Act of the Federal Republic of Germany. This study was approved by the Federal Office for Nature, Environment and Consumer Protection (Landesamt für Natur, Umwelt und Verbraucherschutz, LANU) of North Rhine-Westphalia, Federal Republic of Germany (Approval ID: 84-02.04.2016.A434). For the study, 36 adult female New Zealand white rabbits with a minimum weight of three kilograms were used. Rabbits were randomly allocated into four groups (Figure 1).

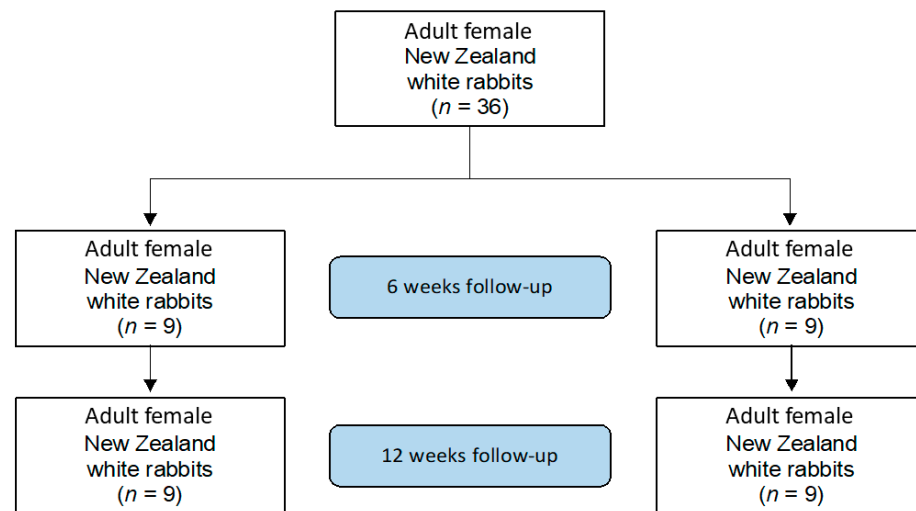


Figure 1. Flow chart of the study set-up.

Before the surgical procedure, general anaesthesia was provided with 0.1 mL/mg/kg bodyweight Medetomidin (Domitor) combined with 0.2 mL Ketamin (Narketan) 10% via subcutaneous injection (Figure 2a,b). The surgical site was shaved, disinfected with iodine and ethanol, and draped in a sterile fashion (Figure 2c). Before incision, 10 mg/kg bodyweight Enrofloxacin was injected subcutaneously. A skin incision was performed over the right lateral femoral condyle (Figure 2d). After preparation through fascia and muscle, the lateral femoral condyle was exposed (Figure 2e). The lateral collateral ligament (LCL) was identified and spared. A unicortical drillhole with a 5.5 mm trephine was prepared under continuous irrigation to avoid thermal necrosis (Figure 2f). After extraction of the bony cylinder (Figure 2g), either a titanium or silanised ceramic cylinder (Figure 2h) was inserted in a press fit fashion (Figure 2i). Attention was given to avoid the lesion of the knee capsule. After irrigation with saline solution, the tissues were closed in layers. Finally, the skin was stapled and sealed with chelated silver spray (Figure 2j). For the first three days after surgery, 4 mg/kg bodyweight Carprofen was applied every 24 h. At 6 and 12 weeks postoperatively, the animals were euthanised with 2 mL/kg bodyweight Natriumpentobarbital (160 mg Natriumpentobarbital/mL), and the femoral condyles were harvested.

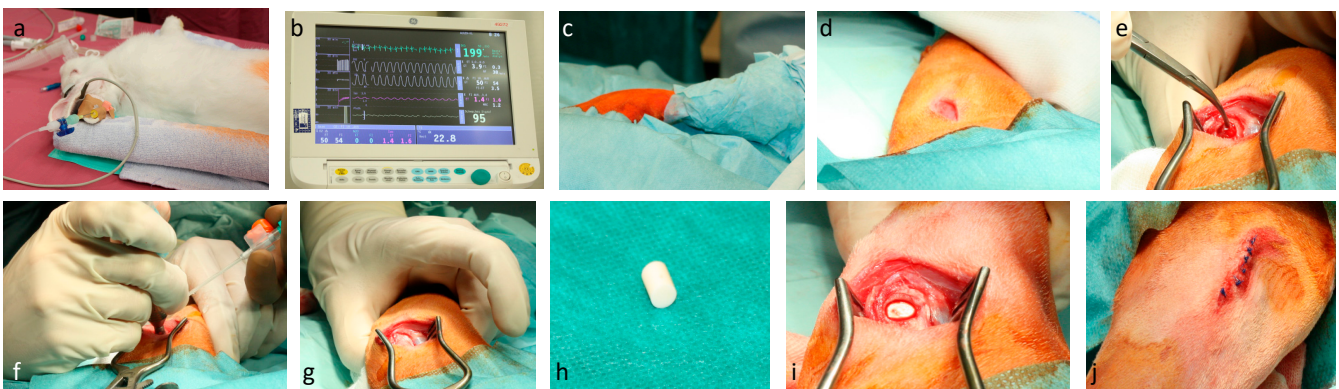


Figure 2. General anaesthesia (a), under monitoring (b), sterile dressed surgical site (c), lateral femoral skin incision (d), preparation of lateral femoral aspect (e), water cooled drilling (f), extraction of the bony cylinder (g), ceramic cylinder (h), sample in situ (i), sutured wound (j).

2.3. Sample Preparation

The femoral condyles were harvested en bloc. Fixation was performed over 12 days with 4% paraformaldehyde followed by an alcohol series with ethanol of 50–100% and xylol. The specimens were embedded in Technovit® 9100 Fa. Heraeus Kulzer. Finally, coplanar thin cuts (60–70 µm) of the specimens were made with a diamond band saw Exakt 300CL. Grinding of titanium implants was performed with sandpaper, whereas silanised ceramics were ground with diamond paper. All specimens were stained with haematoxylin eosin, trichrome, and toluidine. Histomorphometry was conducted by a trained pathologist with an OLYMPUS digital microscope DSX-1000 and stream desktop software (Olympus, Hamburg, Germany).

2.4. Histomorphometry

At microscopic evaluation, the implant sides were divided into four subsections: lateral (K1), distal (K2), medial (K3), and proximal (K4). The region of interest (ROI) represented the percentage of the surrounding area of the implant (red zones) which was analysed (Figure 3).

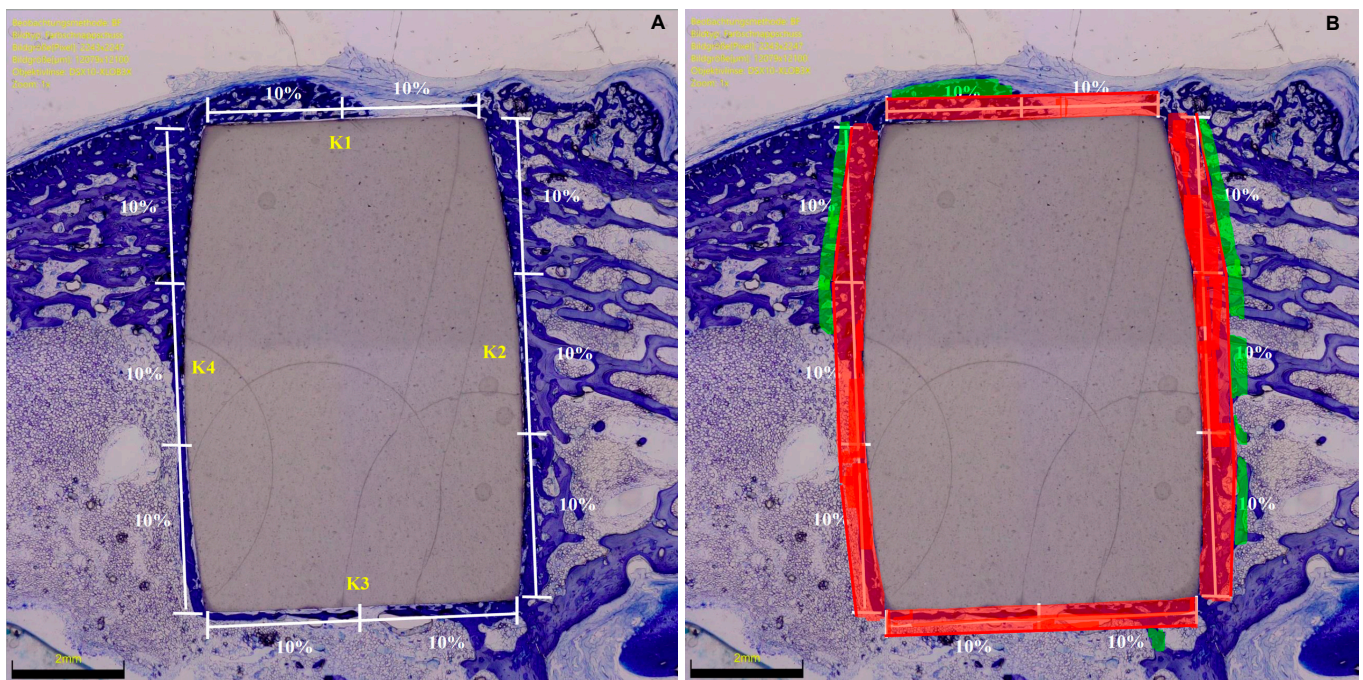


Figure 3. (A) Microscopic evaluation strategy of the BIC: K2 and K4 (longer sides) accounted for 60% (30% each) and the K1 and K3 (shorter sides) for 40% (20% each). (B) Region of interest.

Bone density was measured within each ROI by evaluating the percentage of area filled with mineralized bone. The percentage of ROI covered by immature and unmineralized bone matrix, the osteoid implant contact (OIC), was also quantified (Figure 4). Mature bone implant contact (BIC) was assessed by analysing the length of mineralized bone with direct implant contact as a percentage (Figure 3). The presence of bone resorption, necrosis, and/or inflammation were quantitatively identified and classified: 0 (none), 1 (minimal), 2 (low), 3 (moderate), and 4 (severe).

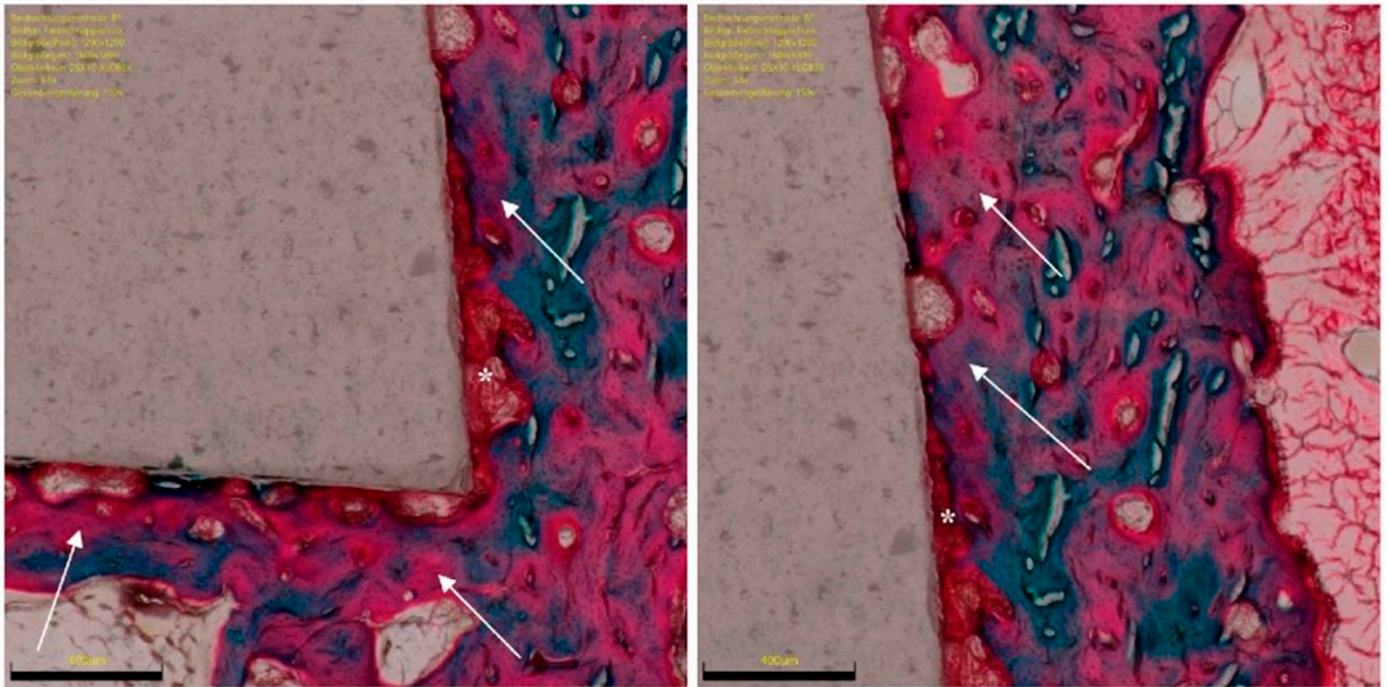


Figure 4. RGD functionalised ceramic implant with surrounding new bone formation (green to pink, arrows), resident bone (green) and osteoid (red, *), adjacent soft tissue. Section preparations in trichrome staining, each magnified 150 \times .

2.5. Outcomes of Interests

We aimed to investigate the potential of osseointegration of ceramic RGD enhanced implants in comparison to standard titanium implants. Hence, OIC, BIC, and the presence of bone necrosis, bone resorption, and/or inflammation in the ROI were quantitatively assessed.

2.6. Statistical Analysis

The IBM SPSS (version 25) was used for the statistical analyses. For descriptive statistics, mean and standard deviation were calculated. For continuous data comparison, the mean difference effect measure was adopted, with standard error (SE) and T-value. The confidence interval (CI) was set at 95% in all the comparisons. The *t*-test was performed, with values of $p < 0.05$ considered statistically significant.

3. Results

All 36 rabbits survived the experimental period of 6 and 12 weeks. No wound dehiscence was reported. At euthanasia, no clinical signs of inflammation or adverse tissue reactions were observed. All implants remained in situ. At baseline, rabbits had a mean weight of 3456.2 ± 243.4 mg. At the last follow-up, rabbits had a mean weight of 4001.8 ± 345.6 mg ($+545.6$ mg; $p < 0.0001$).

3.1. Ossification from 6- to 12-Weeks Follow-up of the RGD Enhanced Implants

No necrosis, bone resorption or inflammation were found in any sample. At 12 weeks follow-up, the overall mean BIC ($p = 0.003$) and IOC ($p = 0.03$) were improved compared to the mean values at 6 weeks (Table 1).

Table 1. Ossification potential of RGD enhanced implants from 6- to 12-weeks (BIC: bone implant contact; OIC: osteoid implant contact; MD: mean difference; CI: confidence interval; SE: standard error).

Endpoint		6 Weeks	12 Weeks	MD	95% CI	SE	t Value	p
Lateral	BIC (%)	3.1 ± 3.4	3.9 ± 1.3	0.8	−0.41 to 2.01	0.61	1.32	0.2
	OIC (%)	0.9 ± 1.2	0.5 ± 0.9	−0.4	−0.90 to 0.10	0.25	−1.60	0.1
Distal	BIC (%)	12.1 ± 4.6	14.3 ± 5.8	2.2	−0.26 to 4.66	1.23	1.78	0.08
	OIC (%)	3.4 ± 3.0	6.0 ± 4.7	2.6	0.75 to 4.45	0.93	2.80	0.007
Medial	BIC (%)	6.8 ± 4.2	8.6 ± 3.2	1.8	0.05 to 3.56	0.88	2.05	0.04
	OIC (%)	3.2 ± 3.2	4.6 ± 4.3	1.4	−0.38 to 3.18	0.89	1.57	0.1
Proximal	BIC (%)	12.6 ± 3.5	13.1 ± 3.5	0.5	−1.14 to 2.14	0.83	0.61	0.5
	OIC (%)	5.0 ± 0.0	5.6 ± 1.8	0.6	0.00 to 1.20	0.30	2.00	0.05
Overall	BIC (%)	34.6 ± 7.9	39.9 ± 6.9	5.3	1.81 to 8.78	1.75	3.03	0.003
	OIC (%)	12.6 ± 6.0	16.8 ± 9.3	4.2	0.52 to 7.87	1.85	2.28	0.03

3.2. Comparison of RGD Enhanced Versus Titanium Implants

At 6 weeks follow-up, the overall OIC was greater in the RGD enhanced group compared to the titanium implant ($p = 0.01$) (Appendix A Table A1). The other endpoints of interest were similar between the two implants at all follow-ups ($p \geq 0.05$). The results of the quantitative analyses are shown in detail in Table 2.

Table 2. Comparison of RGD enhanced versus titanium at 6- and 12-weeks follow-up (MD: mean difference). Negative mean difference indicates greater ossification in favour of the titanium group.

Endpoint		6 Weeks		12 Weeks	
		MD	p	MD	p
Lateral	BIC (%)	0.0	0.5	−1.0	0.05
	OIC (%)	0.9	0.02	1.1	0.4
Distal	BIC (%)	0.6	0.4	0.2	0.4
	OIC (%)	1.9	0.1	0.6	0.3
Medial	BIC (%)	1.5	0.2	1.1	0.05
	OIC (%)	3.5	0.004	1.3	0.05
Proximal	BIC (%)	1.7	0.3	1.0	0.4
	OIC (%)	0.0	1.0	0.7	0.09
Overall	BIC (%)	0.0	0.3	0.0	0.4
	OIC (%)	6.3	0.01	5.7	0.1

4. Discussion

Ceramic implants have several advantages, such as their high hardness and wear resistance, light weight, low modulus of elasticity, outstanding resistance to creep and compressive stress, and no artefacts at imaging [10–12]. Functionalised ceramics with RGD biologically activate the implant surface, enhancing the interaction at the bone implant interface, thus preserving the overall structure and characteristics of the ceramic. The present study confirmed our hypothesis that functionalised ceramic implants enhanced with peptide RGD promote in vivo ossification (Figures 5 and 6). The overall osteoid and bone implant contact improved significantly from 6 to 12 weeks. Finally, RGD enhanced ceramics promoted faster osteoid implant contact in vivo than titanium implants. Overall, the amount of ossification at 12 weeks is comparable between the two implants. No necrosis, bone resorption, or inflammation was observed in any sample at any follow-up.

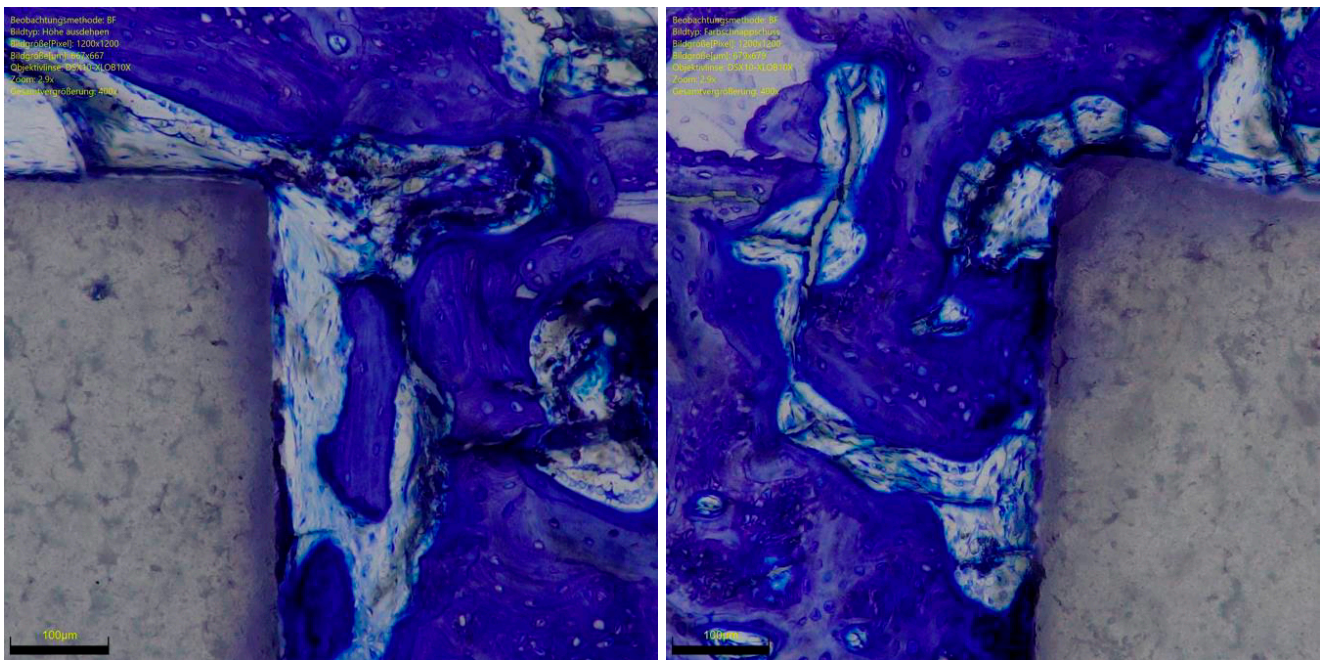


Figure 5. ROI of RGD functionalised ceramic implant with toluidine blue. Contour irregularities and porosities colonised by osteoblasts and osteocytes.

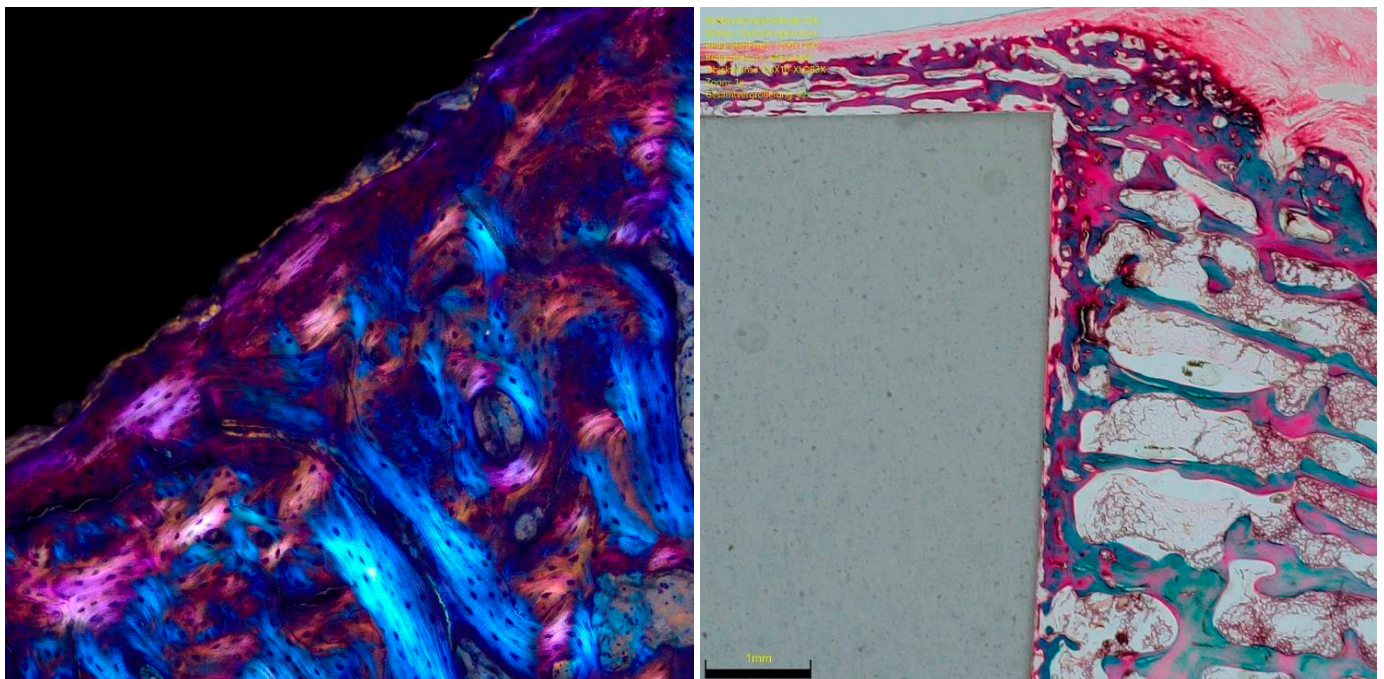


Figure 6. **Left:** Titanium implant in polarised light toluidine blue staining with adjacent newly formed bone, polarised optically magenta-orange and local bone blue. **Right:** RGD functionalised ceramic implant in trichrome staining with adjacent new bone formation in red-green and local bone in green.

The overall BIC improved from 6 to 12 weeks. This improvement was especially evident around the medial and distal portions of the bone implant interface. We hypothesised that the proximity to the cortical bone of the medial epicondyle may stimulate greater new bone formation. This assumption is also supported by the greater osteoid bone formation in this area. The vascular supply of the distal femur in rabbits arises from the epiphyseal

vessels, and the epicondyle is supplied by arteries from the intercondylar notch and epicondyle regions [30,31]. This favours the blood supply into the distal part of the epicondyle, and, given its terminal anatomy, impairs the vascularisation of the distal epiphysis.

Bone is dynamic and undergoes several changes and adaptations. In end stage degenerative or traumatic ailments, implants are commonly used to restore function. Such implants can be permanent or temporary. In case of permanent implants (e.g., arthroplasty), bone integration of the implant to the surrounding bone is crucial to ensure their longevity. The interaction between bones and surrounding tissue is continually regulated by a variety of complex mechanisms. Bone marrow ensures the maintenance of the modelling processes within the bone by regulating cellular migration [32]. Depending on the physical and chemical properties, a foreign body (such as an implant in bone tissue) may produce an immune response [33–35]. The coagulation cascade, the activation of the complement system, and the activation of platelets and immune cells are critical in regulating immune response [36–44]. Coagulation and complement interact synergistically and modulate the initial contact with the surface of the biomaterial [45]. In addition to the immediate immunological reaction, the interaction of implants and bone tissue undergo sequential phases: (1) adsorption of serum and proteins to the implant surface immediately after implantation, activation, proliferation, and adhesion of mesenchymal stem cells and the production of extracellular matrix; (2) osteogenic differentiation of the adhesive mesenchymal stem cells; and (3) calcification of the matrix and the remodelling of the newly formed bone based on the applied loads [35]. The mesenchymal stem cells adhere mainly to the RGD sequences located within the adsorbed proteins, which serve as ligands for the integrin contained within the phospholipidic membrane [46]. The amino acid sequence consisting of arginine (R), glycine (G), and aspartic acid (D) bind the α and β subunits of the trans-membrane heterodimeric integrin [47–50]. The intracellular signalling pathway activated by the RGD integrin binding is extremely varied [51]. Among them, the non-receptor tyrosine kinase FAK (Focal Adhesion Kinase, also PTK2) is activated [52,53], and influences the adhesion of the cell on the extracellular matrix and cell motility in a phosphorylated status. These features may explain the faster osteoid implant integration observed in the first six weeks of the RGD functionalised ceramics.

Several coating processes to functionalise the surface of ceramic have been developed with promising pre-clinical and clinical results [54–57]. Previous studies conducted in rabbit models used heterogeneous coating methodologies, follow-up, analyses, and implantation sites (Table 3). The current evidence on the clinical applications of functionalised ceramic is still limited, and translational studies are required to clarify the best coating process.

Our results confirmed that the *in vivo* osteointegration was similar to that of the titanium implants. However, these results must be considered in light of some limitations. Firstly, between-species differences in histology, cytology, and functional anatomy may impact the reliability of the clinical applicability of our conclusions. The translational potential of each animal model to human clinical conditions is different; however, being reproducible, low cost, and easy to handle, rabbits are one of the most used animal models for *in vivo* experimentations. Biomechanical evaluation of the bone formed—which could provide a comprehensive understanding of bone repair—was not conducted. In the present study, the specimens were stained with haematoxylin eosin, trichrome, and toluidine. Further investigations are needed to evaluate dynamic new bone formation using other methodologies, for example fluorescent with calcein green. Only female rabbits were included in the present investigation. This may introduce biases and between-gender differences were not considered. These results encourage further translational studies to validate our findings in a clinical setting.

Table 3. Previous studies conducted on rabbit models investigating ceramic coating methodologies. Risedronate Calcium Phosphate Silicate Cements (RA-CPSC), Mesoporous silica (SBA15), monocalcium phosphate (MCP), polymerase chain reaction (PCR), Parathyroid hormone-related protein (PTHrP), Adiponectin (APN), Hydroxyapatite (HA), phosphate-buffered saline (PBS), TiO₂ nanotube (TNT), hydroxyapatite-TiO₂ nanotube (TNT-HA), calcium phosphate ceramic (CPC), poly(ϵ -caprolactone) (PCL), tricalcium phosphate 70% (TCP).

Author, Year	Rabbit Model	Rabbits (n) and Implant Site	Materials	Follow-Up	Type of Analyses
Gong et al., 2016 [58]	30 New Zealand rabbits	Right medial tibia epiphysis of the ($d = 6$ mm, $\phi = 3$ mm)	Calcium silicate powder, RA-CPSC, MCP, Ca(H ₂ PO ₄) ₂ , and risedronate added into calcium silicate powder and homogeneously mixed, respectively.	8, 10 weeks	X-ray semi-quantitative analysis; PCR
Lozano et al., 2012 [59]	Osteoporosis induced rabbits	Medial and lateral distal femoral epiphysis	SBA15 and SiO ₂ . The surface was chemically modified with an organic modification of silica walls with alkoxysilane, <i>n</i> -octyltriethoxysilane and functionalized by soaking the mesoporous in a solution of PTHrP in PBS.	2 weeks	Histology; Immunohistochemistry
Luo et al., 2012 [60]	60 New Zealand rabbits	Sub-periosteal mandibular (4 mm \times 5 mm \times 10 mm)	Porous commercial HA was physically functionalized in surface with or without APN or Matrigel or combination of both.	4 weeks	Micro-CT; Biomechanical analyses
Plaza et al., 2016 [61]	42 New Zealand white rabbits	Medial femoral condyles A	Physical incorporation of fibronectin in HA bulk material by adding HA to a fibronectin solution of in PBS.	1, 2, 5 days	Micro-CT; Histology
Shen et al. 2016 [62]	43 New Zealand white rabbits	Femoral epiphysis	TNT were immersed in supersaturated Ca(OH) ₂ solution, Ca(NO ₃) ₂ ·4H ₂ O (0.2 M) and (NH ₄) ₂ HPO ₄ (0.2 M) solutions to create a coating of HA. TNT-HA was subsequently functionalized with Aln by immersion in Aln solution (physical absorption).	12 weeks	X-rays; Micro-CT; Biomechanical analyses; Histology
Wu et al., 2015 [63]	16 New Zealand White rabbits	Distal femur	Strontium enriched CPC in the solid phase and PCL.	24 weeks	Micro-CT
Yu et al., 2017 [64]	40 New Zealand white rabbits	Two implants (2 mm diameter, 10 mm depth) into each femur	Ti-6Al-4V implants ($\phi 10 \times 2$ mm) coated by means of plasma-spray technique with HA or CaSiO ₃ or zinc-modified calcium silicate (Ca ₂ ZnSi ₂ O ₇) at two different Zn contents.	4, 8, 12 weeks	Micro-CT; Histology
Gunnella et al., 2017 [65]	30 California rabbits	Not specified (5 mm wide and 4 mm)	A composite material of HA/TCP granules with or without Sr substitution.	12 weeks	Histomorphometry; Immunohistochemistry

5. Conclusions

Functionalised ceramic enhanced with RGD peptide promoted *in vivo* osteointegration. The overall osteoid and bone implant contact improved significantly from 6 to 12 weeks. Finally, RGD enhanced ceramics promoted faster osteoid implant contact *in vivo* than titanium implants. Overall, the amount of osteointegration at 12 weeks is comparable with that of titanium implants. No necrosis, bone resorption or inflammation was observed in any sample at any follow-up point.

Author Contributions: Conceptualization, F.M.; Investigation, H.S. and J.E.; Project administration, N.M.; Supervision, F.H.; Writing—original draft, F.M. All authors have read and agreed to the published version of the manuscript.

Funding: This research was funded by the German Federal Ministry of Education and Research (Bundesministerium für Bildung und Forschung, BMBF) Funding as part of the Validation of the Technological and Social Innovation Potential of Scientific Research (Validierung des Technologischen und Gesellschaftlichen Innovationspotenzials wissenschaftlicher Forschung).

Institutional Review Board Statement: This study was conducted according to the Animal Welfare Act of the Federal Republic of Germany. This study was approved by the Federal Office for Nature, Environment and Consumer Protection (Landesamt für Natur, Umwelt und Verbraucherschutz, LANU) of North Rhine-Westphalia, Federal Republic of Germany (Approval ID: 84-02.04.2016.A434).

Informed Consent Statement: Not applicable.

Data Availability Statement: The data presented in this study are available on request from the corresponding author.

Conflicts of Interest: The authors declare no conflict of interest.

Appendix A

Table A1. Ossification potential of titanium implants at 6- and 12-weeks (BIC: bone implant contact; OIC: osteoid implant contact).

Endpoint		6 Weeks	12 Weeks
Lateral	BIC (%)	3.1 ± 4.1	4.9 ± 4.6
	OIC (%)	0	−1.4 ± 0.8
Distal	BIC (%)	11.5 ± 2.3	14.1 ± 8.1
	OIC (%)	1.5 ± 3.0	5.4 ± 4.1
Medial	BIC (%)	5.3 ± 3.4	7.5 ± 2.1
	OIC (%)	−0.3 ± 0.7	3.3 ± 2.0
Proximal	BIC (%)	10.9 ± 9.1	12.1 ± 3.7
	OIC (%)	5.0 ± 0.3	4.9 ± 1.9
Overall	BIC (%)	34.6 ± 15.1	39.9 ± 19.3
	OIC (%)	6.3 ± 2.4	11.1 ± 6.5

References

- Pilliar, R.M. Metallic Biomaterials. In *Biomedical Materials*; Narayan, R.C., Ed.; Springer Science+Business Media, LLC: Berlin/Heidelberg, Germany, 2009; Volume 2, pp. 41–81.
- Kaur, M.; Singh, K. Review on titanium and titanium based alloys as biomaterials for orthopaedic applications. *Mater. Sci. Eng. C Mater. Biol. Appl.* **2019**, *102*, 844–862. [[CrossRef](#)] [[PubMed](#)]
- Bosshardt, D.D.; Chappuis, V.; Buser, D. Osseointegration of titanium, titanium alloy and zirconia dental implants: Current knowledge and open questions. *Periodontology 2000* **2017**, *73*, 22–40. [[CrossRef](#)] [[PubMed](#)]
- Pacheco, K.A. Allergy to Surgical Implants. *Clin. Rev. Allergy Immunol.* **2019**, *56*, 72–85. [[CrossRef](#)] [[PubMed](#)]
- Swiatkowska, I.; Martin, N.G.; Henckel, J.; Apthorp, H.; Hamshere, J.; Hart, A.J. Blood and plasma titanium levels associated with well-functioning hip implants. *J. Trace Elements Med. Biol.* **2020**, *57*, 9–17. [[CrossRef](#)]
- Teo, W.Z.W.; Schalock, P.C. Metal Hypersensitivity Reactions to Orthopedic Implants. *Dermatol. Ther.* **2017**, *7*, 53–64. [[CrossRef](#)]
- Kretzer, J.P.; Reinders, J.; Sonntag, R.; Hagmann, S.; Streit, M.; Jeager, S.; Moradi, B. Wear in total knee arthroplasty—Just a question of polyethylene? Metal ion release in total knee arthroplasty. *Int. Orthop.* **2014**, *38*, 335–340. [[CrossRef](#)]

8. Solarino, G.; Piconi, C.; De Santis, V.; Piazzolla, A.; Moretti, B. Ceramic Total Knee Arthroplasty: Ready to Go? *Joints* **2017**, *5*, 224–228. [[CrossRef](#)]
9. Middleton, S.; Toms, A. Allergy in total knee arthroplasty: A review of the facts. *Bone Jt. J.* **2016**, *98-B*, 437–441. [[CrossRef](#)]
10. Zhang, L.; Haddouti, E.-M.; Welle, K.; Burger, C.; Kabir, K.; Schildberg, F.A. Local Cellular Responses to Metallic and Ceramic Nanoparticles from Orthopedic Joint Arthroplasty Implants. *Int. J. Nanomed.* **2020**, *15*, 6705–6720. [[CrossRef](#)]
11. Trieb, K.; Glinz, J.; Reiter, M.; Kastner, J.; Senck, S. Non-Destructive Testing of Ceramic Knee Implants Using Micro-Computed Tomography. *J. Arthroplast.* **2019**, *34*, 2111–2117. [[CrossRef](#)]
12. Li, C.; Ai, F.; Miao, X.; Liao, H.; Li, F.; Liu, M.; Yu, F.; Dong, L.; Li, T.; Wang, X. “The return of ceramic implants”: Rose stem inspired dual layered modification of ceramic scaffolds with improved mechanical and anti-infective properties. *Mater. Sci. Eng. C Mater. Biol. Appl.* **2018**, *93*, 873–879. [[CrossRef](#)] [[PubMed](#)]
13. Vladescu, A.; Cotrut, C.M.; Azem, F.A.; Bramowicz, M.; Pana, I.; Braic, V.; Birlik, I.; Kiss, A.; Braic, M.; Abdulgader, R.; et al. Sputtered Si and Mg doped hydroxyapatite for biomedical applications. *Biomed. Mater.* **2018**, *13*, 025011. [[CrossRef](#)] [[PubMed](#)]
14. Zhang, P.; Wang, X.; Lin, Z.; Lin, H.; Zhang, Z.; Li, W.; Yang, X.; Cui, J. Ti-Based Biomedical Material Modified with TiO_x/TiN_x Duplex Bioactivity Film via Micro-Arc Oxidation and Nitrogen Ion Implantation. *Nanomaterials* **2017**, *7*, 343. [[CrossRef](#)] [[PubMed](#)]
15. Duncan, W.J.; Lee, M.-H.; Bae, T.-S.; Lee, S.-J.; Gay, J.; Loch, C. Anodisation Increases Integration of Unloaded Titanium Implants in Sheep Mandible. *BioMed Res. Int.* **2015**, *2015*, 857969. [[CrossRef](#)]
16. Song, C.; Wang, S.; Liu, J.; Zhai, S. Microstructure and Mechanical Properties of Al₂O₃/Er₃Al₅O₁₂ Binary Eutectic Ceramic Prepared by Bridgman Method. *Materials* **2018**, *11*, 534. [[CrossRef](#)]
17. Denes, E.; Barrière, G.; Poli, E.; Lévêque, G. Alumina Biocompatibility. *J. Long-Term Eff. Med. Implant.* **2018**, *28*, 9–13. [[CrossRef](#)]
18. Kim, S.-E.; Cho, W.-J.; Yoon, J.-K.; Shon, I.-J. The Effect of BN Reinforcement on the Mechanical Properties of Nanostructured Al₂O₃ Ceramics. *J. Nanosci. Nanotechnol.* **2020**, *20*, 4353–4357. [[CrossRef](#)]
19. Chugunov, S.; Adams, N.A.; Akhatov, I.S. Evolution of SLA-Based Al₂O₃ Microstructure During Additive Manufacturing Process. *Materials* **2020**, *13*, 3928. [[CrossRef](#)]
20. Agarwal, R.; García, A.J. Biomaterial strategies for engineering implants for enhanced osseointegration and bone repair. *Adv. Drug Deliv. Rev.* **2015**, *94*, 53–62. [[CrossRef](#)]
21. Shao, Z.; Zhang, X.; Pi, Y.; Wang, X.; Jia, Z.; Zhu, J.; Dai, L.; Chen, W.; Yin, L.; Chen, H.; et al. Polycaprolactone electrospun mesh conjugated with an MSC affinity peptide for MSC homing in vivo. *Biomaterials* **2012**, *33*, 3375–3387. [[CrossRef](#)]
22. Cho, H.; Balaji, S.; Sheikh, A.Q.; Hurley, J.R.; Tian, Y.F.; Collier, J.H.; Crombleholme, T.M.; Narmoneva, D.A. Regulation of endothelial cell activation and angiogenesis by injectable peptide nanofibers. *Acta Biomater.* **2012**, *8*, 154–164. [[CrossRef](#)] [[PubMed](#)]
23. Böke, F.; Giner, I.; Keller, A.; Grundmeier, G.; Fischer, H. Plasma-Enhanced Chemical Vapor Deposition (PE-CVD) yields better Hydrolytical Stability of Biocompatible SiO_x Thin Films on Implant Alumina Ceramics compared to Rapid Thermal Evaporation Physical Vapor Deposition (PVD). *ACS Appl. Mater. Interfaces* **2016**, *8*, 17805–17816. [[CrossRef](#)] [[PubMed](#)]
24. Vasudev, M.C.; Anderson, K.D.; Bunning, T.J.; Tsukruk, V.V.; Naik, R.R. Exploration of Plasma-Enhanced Chemical Vapor Deposition as a Method for Thin-Film Fabrication with Biological Applications. *ACS Appl. Mater. Interfaces* **2013**, *5*, 3983–3994. [[CrossRef](#)] [[PubMed](#)]
25. Li, Y.; Ren, J.; Wang, B.; Lu, W.; Wang, H.; Hou, W. Development of biobased multilayer films with improved compatibility between polylactic acid-chitosan as a function of transition coating of SiO_x. *Int. J. Biol. Macromol.* **2020**, *165*, 1258–1263. [[CrossRef](#)] [[PubMed](#)]
26. Kim, J.Y.; Sung, G.Y.; Park, M. Efficient Portable Urea Biosensor Based on Urease Immobilized Membrane for Monitoring of Physiological Fluids. *Biomedicines* **2020**, *8*, 596. [[CrossRef](#)]
27. Si, Y.J.; Ren, Q.H.; Bi, L. miR-135b-5p regulates human mesenchymal stem cell osteogenic differentiation by facilitating the Hippo signaling pathway. *Int. J. Clin. Exp. Pathol.* **2017**, *10*, 7767–7775.
28. Walker, J.M. The bicinchoninic acid (BCA) assay for protein quantitation. *Methods Mol. Biol.* **1994**, *32*, 5–8. [[CrossRef](#)]
29. Böke, F.; Labude, N.; Lauria, I.; Ernst, S.; Müller-Newen, G.; Neuss, S.; Fischer, H. Biological Activation of Bioinert Medical High-Performance Oxide Ceramics by Hydrolytically Stable Immobilization of c(RGDyK) and BMP-2. *ACS Appl. Mater. Interfaces* **2018**, *10*, 38669–38680. [[CrossRef](#)]
30. Doschak, M.R.; Cooper, D.M.L.; Huculak, C.N.; Matyas, J.R.; Hart, D.A.; Hallgrímsson, B.; Zernicke, R.F.; Bray, R.C. Angiogenesis in the distal femoral chondroepiphysis of the rabbit during development of the secondary centre of ossification. *J. Anat.* **2003**, *203*, 223–233. [[CrossRef](#)]
31. Alberty, A. Effects of Physeal Distraction on the Vascular Supply of the Growth Area: A microangiographical study in rabbits. *J. Pediatr. Orthop.* **1993**, *13*, 373–377. [[CrossRef](#)]
32. Wegst, U.G.; Bai, H.; Saiz, E.; Tomsia, A.P.; Ritchie, R.O. Bioinspired structural materials. *Nat. Mater.* **2015**, *14*, 23–36. [[CrossRef](#)] [[PubMed](#)]
33. Anderson, J.M.; Rodriguez, A.; Chang, D.T. Foreign body reaction to biomaterials. *Semin. Immunol.* **2008**, *20*, 86–100. [[CrossRef](#)] [[PubMed](#)]
34. Franz, S.; Rammelt, S.; Scharnweber, D.; Simon, J.C. Immune responses to implants—A review of the implications for the design of immunomodulatory biomaterials. *Biomaterials* **2011**, *32*, 6692–6709. [[CrossRef](#)] [[PubMed](#)]

35. Puleo, D.A.; Nanci, A. Understanding and controlling the bone-implant interface. *Biomaterials* **1999**, *20*, 2311–2321. [[CrossRef](#)]
36. Lhotta, K.; Würzner, R.; Kronenberg, F.; Oppermann, M.; König, P. Rapid activation of the complement system by cuprophane depends on complement component C4. *Kidney Int.* **1998**, *53*, 1044–1051. [[CrossRef](#)]
37. Hed, J.; Johansson, M.; Lindroth, M. Complement activation according to the alternate pathway by glass and plastic surfaces and its role in neutrophil adhesion. *Immunol. Lett.* **1984**, *8*, 295–299. [[CrossRef](#)]
38. Wilson, C.J.; Clegg, R.E.; Leavesley, D.I.; Pearcy, M.J. Mediation of Biomaterial-Cell Interactions by Adsorbed Proteins: A Review. *Tissue Eng.* **2005**, *11*, 1–18. [[CrossRef](#)]
39. Zhuo, R.; Siedlecki, C.A.; Vogler, E.A. Autoactivation of blood factor XII at hydrophilic and hydrophobic surfaces. *Biomaterials* **2006**, *27*, 4325–4332. [[CrossRef](#)]
40. Kalltorp, M.; Askendal, A.; Thomsen, P.; Tengvall, P. Ellipsometric studies in vitro on kinetics of rat complement activation. *J. Biomed. Mater. Res.* **1999**, *44*, 222–225. [[CrossRef](#)]
41. Sarma, J.V.; Ward, P.A. The complement system. *Cell Tissue Res.* **2011**, *343*, 227–235. [[CrossRef](#)]
42. Gorbet, M.B.; Sefton, M.V. Biomaterial-associated thrombosis: Roles of coagulation factors, complement, platelets and leukocytes. *Biomaterials* **2004**, *25*, 5681–5703. [[CrossRef](#)] [[PubMed](#)]
43. Johnson, R.J. Complement activation during extracorporeal therapy: Biochemistry, cell biology and clinical relevance. *Nephrol. Dial. Transpl.* **1994**, *9* (Suppl. 2), 36–45.
44. Giorgetti, A.; Marchetto, M.C.N.; Li, M.; Yu, D.; Fazzina, R.; Mu, Y.; Adamo, A.; Paramonov, I.; Cardoso, J.C.; Monasterio, M.B.; et al. Cord blood-derived neuronal cells by ectopic expression of Sox2 and c-Myc. *Proc. Natl. Acad. Sci. USA* **2012**, *109*, 12556–12561. [[CrossRef](#)] [[PubMed](#)]
45. Fischer, M.; Sperling, C.; Werner, C. Synergistic effect of hydrophobic and anionic surface groups triggers blood coagulation in vitro. *J. Mater. Sci. Mater. Med.* **2010**, *21*, 931–937. [[CrossRef](#)]
46. Salasznyk, R.M.; Williams, W.A.; Boskey, A.; Batorsky, A.; Plopper, G.E. Adhesion to Vitronectin and Collagen I Promotes Osteogenic Differentiation of Human Mesenchymal Stem Cells. *J. Biomed. Biotechnol.* **2004**, *2004*, 24–34. [[CrossRef](#)]
47. Xiong, J.-P.; Stehle, T.; Diefenbach, B.; Zhang, R.; Dunker, R.; Scott, D.L.; Joachimiak, A.; Goodman, S.L.; Arnaout, M.A. Crystal Structure of the Extracellular Segment of Integrin $\alpha V\beta 3$. *Science* **2001**, *294*, 339–345. [[CrossRef](#)]
48. Xiao, T.; Takagi, J.; Collier, B.S.; Wang, J.-H.; Springer, T.A. Structural basis for allostery in integrins and binding to fibrinogen-mimetic therapeutics. *Nature* **2004**, *432*, 59–67. [[CrossRef](#)]
49. Hynes, R.O. Integrins: Bidirectional, Allosteric Signaling Machines. *Cell* **2002**, *110*, 673–687. [[CrossRef](#)]
50. Danen, E.; Sonnenberg, A. Erratum: Integrins in regulation of tissue development and function. *J. Pathol.* **2003**, *201*, 632–641. [[CrossRef](#)]
51. Humphries, J.D.; Byron, A.; Humphries, M.J. Integrin ligands at a glance. *J. Cell Sci.* **2006**, *119* (Pt 19), 3901–3903. [[CrossRef](#)]
52. Zachary, I.; Rozengurt, E. Focal adhesion kinase (p125FAK): A point of convergence in the action of neuropeptides, integrins, and oncogenes. *Cell* **1992**, *71*, 891–894. [[CrossRef](#)]
53. Abedi, H.; Zachary, I. Vascular Endothelial Growth Factor Stimulates Tyrosine Phosphorylation and Recruitment to New Focal Adhesions of Focal Adhesion Kinase and Paxillin in Endothelial Cells. *J. Biol. Chem.* **1997**, *272*, 15442–15451. [[CrossRef](#)] [[PubMed](#)]
54. Aro, H.T.; Alm, J.J.; Moritz, N.; Mäkinen, T.J.; Lankinen, P. Low BMD affects initial stability and delays stem osseointegration in cementless total hip arthroplasty in women: A 2-year RSA study of 39 patients. *Acta Orthop.* **2012**, *83*, 107–114. [[CrossRef](#)] [[PubMed](#)]
55. Lee, Y.-K.; Ha, Y.-C.; Chang, B.-K.; Kim, K.-C.; Kim, T.-Y.; Koo, K.-H. Cementless Bipolar Hemiarthroplasty Using a Hydroxyapatite-Coated Long Stem for Osteoporotic Unstable Intertrochanteric Fractures. *J. Arthroplast.* **2011**, *26*, 626–632. [[CrossRef](#)]
56. Tao, Z.; Zhou, W.; Jiang, Y.; Wu, X.; Xu, Z.; Yang, M.; Xie, J. Effects of strontium-modified calcium phosphate cement combined with bone morphogenetic protein-2 on osteoporotic bone defects healing in rats. *J. Biomater. Appl.* **2018**, *33*, 3–10. [[CrossRef](#)]
57. Tao, Z.-S.; Zhou, W.-S.; He, X.-W.; Liu, W.; Bai, B.-L.; Zhou, Q.; Huang, Z.-L.; Tu, K.-K.; Li, H.; Sun, T.; et al. A comparative study of zinc, magnesium, strontium-incorporated hydroxyapatite-coated titanium implants for osseointegration of osteopenic rats. *Mater. Sci. Eng. C Mater. Biol. Appl.* **2016**, *62*, 226–232. [[CrossRef](#)]
58. Gong, T.; Chen, Y.; Zhang, Y.; Zhang, Y.; Liu, X.; Troczynski, T.; Häfeli, U.O. Osteogenic and anti-osteoporotic effects of risedronate-added calcium phosphate silicate cement. *Biomed. Mater.* **2016**, *11*, 045002. [[CrossRef](#)]
59. Lozano, D.; Trejo, C.G.; Gómez-Barrena, E.; Manzano, M.; Doadrio, J.C.; Salinas, A.J.; Vallet-Regí, M.; García-Honduvilla, N.; Esbrit, P.; Buján, J. Osteostatin-loaded onto mesoporous ceramics improves the early phase of bone regeneration in a rabbit osteopenia model. *Acta Biomater.* **2012**, *8*, 2317–2323. [[CrossRef](#)]
60. Luo, E.; Hu, J.; Bao, C.; Li, Y.; Tu, Q.; Murray, D.; Chen, J. Sustained release of adiponectin improves osteogenesis around hydroxyapatite implants by suppressing osteoclast activity in ovariectomized rabbits. *Acta Biomater.* **2012**, *8*, 734–743. [[CrossRef](#)]
61. Plaza, J.Q.; Garzón, L.B.; Gimenez, B.B.; Moraleda, B.F.; Collía, F.; Rodríguez-Lorenzo, L.M. Application of calcium phosphates and fibronectin as complementary treatment for osteoporotic bone fractures. *Injury* **2016**, *47*, 15–21. [[CrossRef](#)]
62. Shen, X.; Ma, P.; Hu, Y.; Xu, G.; Xu, K.; Chen, W.; Ran, Q.; Dai, L.; Yu, Y.; Mu, C.; et al. Alendronate-loaded hydroxyapatite-TiO₂ nanotubes for improved bone formation in osteoporotic rabbits. *J. Mater. Chem.* **2016**, *4*, 1423–1436. [[CrossRef](#)] [[PubMed](#)]

63. Wu, C.C.; Kuo, C.L.; Fan, F.Y.; Yang, K.-C. Strontium-impregnated bioabsorbable composite for osteoporotic fracture fixation. *J. Biomed. Mater. Res.* **2015**, *103*, 3355–3363. [[CrossRef](#)] [[PubMed](#)]
64. Yu, J.; Xu, L.; Li, K.; Xie, N.; Xi, Y.; Wang, Y.; Zheng, X.; Chen, X.; Wang, M.; Ye, X. Zinc-modified calcium silicate coatings promote osteogenic differentiation through TGF- β /Smad pathway and osseointegration in osteopenic rabbits. *Sci. Rep.* **2017**, *7*, 3440. [[CrossRef](#)] [[PubMed](#)]
65. Gunnella, F.; Kunisch, E.; Bungartz, M.; Maenz, S.; Horbert, V.; Xin, L.; Mika, J.; Borowski, J.; Bischoff, S.; Schubert, H.; et al. Low-dose BMP-2 is sufficient to enhance the bone formation induced by an injectable, PLGA fiber-reinforced, brushite-forming cement in a sheep defect model of lumbar osteopenia. *Spine J.* **2017**, *17*, 1699–1711. [[CrossRef](#)] [[PubMed](#)]